Multi-Element Probabilistic Collocation for Sensitivity Analysis in Cellular Signaling Networks

Jasmine Foo[±], Suzanne Sindi[†], George Em Karniadakis[‡]

Division of Applied Mathematics

Brown University

Providence, RI 02912 USA

[±]jfoo@dam.brown.edu,[†]ssindi@dam.brown.edu, [‡]gk@dam.brown.edu

October 5, 2009

Abstract

In this work we formulate the Multi-Element Probabilistic Collocation Method (ME-PCM) as a tool for sensitivity analysis of differential equation models as applied to cellular signaling networks. This method utilizes a simple, efficient sampling algorithm to quantify local sensitivities throughout the parameter space. We apply the ME-PCM to a previously published ordinary differential equation model of the apoptosis signaling network. We first verify agreement with the previously identified regions of sensitivity and then go on to analyze this region in greater detail with the ME-PCM. We demonstrate the generality of the ME-PCM by studying sensitivity of the system using a variety of biologically relevant markers in the system such as variation in one (or many) chemical species as a function of time, and total exposure of a single chemical species.

1 Introduction

We introduce a general method of parametric sensitivity analysis that enables investigation of deterministic and stochastic differential equations of cellular signaling networks. Parametric

sensitivity analysis techniques are used to quantify the sensitivity of system outputs to uncertainty in parameters. With these techniques it is possible to reveal the robustness or fragility of a system to variation in certain parameters; this may guide experimental design as well as contribute to the knowledge of a biological system. Many parameter sensitivity analysis techniques have been developed for mathematical models of cellular signaling networks as well as for metabolic control analysis (MCA)[1]. Local (gradient-based) parameter sensitivity analysis techniques have been used to identify important parameters in dynamic models of signal transduction (e.g. [2], [3], [4]) and in metabolic pathways ([5], [4], [6]). These methods all utilize similar gradient-type measures of sensitivity, wherein the sensitivities are defined as derivatives or a normalized change in output per normalized change in input. Recently, more attention has been focused on extending these gradient-based techniques for analyzing sensitivities for non-steady state trajectories ([7], [8]). In many systems it is the transient or oscillatory behaviour which is of primary interest, such as in signal transduction networks. In ([9]) the authors develop a novel method for studying signal-response systems where transient signals determine the biological outcome using Direct finite-time Lyapunov exponents (DLEs). Some additional extensions of metabolic control analysis techniques to non-steady behaviour have appeared in the literature (e.g. in [5]).

Local sensitivity analysis techniques evaluate slopes of the system outputs with respect to each parameter at a particular point in the parameter space. By introducing stochasticity in these parameters, we can quantify the sensitivity of the system to these parameters by calculating statistical properties of the outputs. Then, the sensitivity of the of a system output with respect to the parameter can be measured using statistical or probabilistic analyses of this stochastic system. Thus, stochastic methods present an alternative to local gradient-based techniques and are philosophically different in their definition of sensitivity as we further address in the Discussion. Several stochastic Monte Carlo-type sampling methods have been applied to sensitivity analysis of biological systems (e.g. [10], [11], [12]). These methods are robust and provide important information about system sensitivity, but are often too computationally intensive for studying complex systems where the cost of computing a sufficient number of samples is intractable.

In this paper we propose a general stochastic method, called the Multi-Element Probabilistic Collocation Method (ME-PCM) ([13]), for sensitivity analysis in large-scale cellular signaling

networks. It is based on stochastic spectral methods, a class of numerical methods widely used in engineering applications ([14, 15, 16, 17]) and more recently in biological systems ([18]) in a gradient-based sensitivity approach. In the ME-PCM, uncertain parameters are cast as stochastic quantities in the system and sensitivity of the output is measured in terms of local statistical moments in multidimensional sub-regions of the parametric space. Local variances of the system output provide novel information about the spread of the system outcomes due to simultaneous parameter variation throughout each sub-region. If the variance is low, the system is robust to changes in this parameter sub-region; if the variance is high, the system is highly sensitive in this region, perhaps indicating that further experimental efforts should be focused in this area. The ME-PCM, also an algorithmically simple sampling method like Monte Carlo, has been shown to be much more computationally efficient than Monte-Carlo due to a 'smart' choice of sampling points ([13]). With the ME-PCM we can additionally contribute time-varying sensitivity analysis for systems whose output is determined in transience. Another attractive feature of the ME-PCM is its ability to simultaneously study a variety of measures of sensitivity.

In this manuscript, we apply the ME-PCM to the study of a previously published model of the apoptosis signaling network ([9]). The model we study is a key sub-network in the cellular signaling network determining if a cell should undergo programmed cell death when confronted with a death ligand. In Section 2 we develop the ME-PCM and demonstrate ways of using it to study the sensitivity of the system to a variety of biologically relevant quantities including variation in any number of chemical species concentrations in time, and exposure to individual chemical species. In Section 3 we introduce the model of the apoptosis signaling network and first demonstrate the ME-PCM identifies a similar region of sensitivity as previously reported in [9]. We go on to illustrate the strength of our method; with minimal additional computational effort, we are able to study the region of sensitivity as it emerges and evolves in time as well as the sensitivity of other biologically relevant quantities. We demonstrate that by studying the contribution of each variable to the sensitivity allows us to determine the single variable that contributes the most to the overall global sensitivity. In Section 4 we discuss the advantages and limitations of the ME-PCM, applications to studying biological systems and comparisons between our approach and gradient-based approaches such as the one used in ([9]). In the Appendix, we establish a mathematical connection between variance-based and gradient-based

approaches to sensitivity analysis.

2 Sensitivity Analysis Using the Multi-Element Probabilistic Collocation Method

We begin by describing the Multi-Element Probabilistic Collocation Method (ME-PCM) ([13]), and its application to sensitivity analysis in biological systems. The ME-PCM is an outgrowth of the probabilistic collocation method originally introduced in ([19]) for finding statistical moments of solutions to partial differential equations with random parameters. It is essentially a sampling method, similar to Monte Carlo methods in implementation but with additional pre- and post-processing procedures. Instead of randomly sampling the parameter space, the ME-PCM uses domain decomposition and numerical quadrature rules to sample more efficiently. The inherent generality of the ME-PCM allows us to calculate the sensitivity of a large variety of biologically relevant quantities, and to locate regions of high sensitivity within the parameter space. In the following we describe the process of using this method for sensitivity analysis of a model problem and give some example measures of sensitivity.

For clarity, we formulate the ME-PCM here in the context of studying the sensitivity of a general system of ODEs describing a biochemical system to varying initial conditions and parameters. However, this method is applicable for sensitivity analysis of general PDE and ODE systems with general parametric inputs. Thus, it can be viewed as a sensitivity analysis tool for general differential equation models of biological systems and cellular signaling networks, including systems with spatial dependence and diffusion, for example.

Consider a general model system of equations representing the biochemical pathways of a cellular signaling network with N molecular species. Define $\boldsymbol{x}(t)$ to be a vector of concentrations of each molecular species as a function of time $(x_1(t), x_2(t), ..., x_N(t))$ where $x_i(t)$ is the concentration of the i-th chemical at time t. The ODE model describing the chemical kinetics of this system is given by:

$$\dot{\boldsymbol{x}}(t) = f(\boldsymbol{x}, \boldsymbol{x}_0, t) \tag{1}$$

where $\boldsymbol{x}_0 = (x_1(0), x_2(0), ..., x_N(0))$ denotes the initial conditions of the system. Suppose we are interested in studying the sensitivity of this system to its initial conditions within defined ranges. The initial condition of each chemical x_i is assumed to vary on an interval $[a_i, b_i]$,

and $\Gamma = \prod_i^N [a_i, b_i]$ is defined to be the space of all possible initial condition combinations (i.e. parameter space). Now, define Y_i to be a uniform random variable on the Γ_i for each $i = 1, .., N$ and let $\boldsymbol{Y} = (Y_1, Y_2, ..., Y_N)$. We are interested in quantifying the sensitivity in the following stochastic system:

$$\dot{\boldsymbol{x}}(t) = f(\boldsymbol{x}(t), \boldsymbol{Y}, t). \tag{2}$$

Since the parameters $\boldsymbol{Y}$ are stochastic, the dependent variables $x_1(t), ..., x_N(t)$ are all stochastic as well. In fact, we will explicitly refer to to this dependence as $x_i(t, \boldsymbol{Y})$ often in this paper. The 'random dimension' of the system is defined to be the dimension of the parameter space Γ, or N in this example. The same formulation can also be used to study sensitivity to varying other parameters such as rate constants, by setting them to be random parameters as well.

Using this setup, we next describe the ME-PCM procedure in three steps. During the preprocessing step, the parameter space is discretized and a set of sampling points is chosen. Next, mathematical markers are chosen to characterize biologically relevant quantities. In the last step, the sensitivity of these quantities is evaluated in each region of parameter space.

2.0.1 Step 1: Preprocessing

We first decompose the parameter space Γ into N_e nonoverlapping rectangular elements $\{B^i\}_{i=1}^{N_e}$. In each element B^i, we choose a set of r points $\{\boldsymbol{q}_j^i\}_{j=1}^r$ and weights $\{w_j^i\}_{j=1}^r$, which correspond to a numerical integration (or quadrature) rule over the element such that:

$$\sum_{j=1}^{r} g(\boldsymbol{q}_j^i) w_j^i \approx \int_{B^i} g(\boldsymbol{x}) d\boldsymbol{x} \tag{3}$$

for g in a class of functions specified by the quadrature rule. These quadrature points will prescribe the sampling locations later in the procedure. We consider two main types of multi-dimensional numerical integration rules: tensor-product Gaussian quadrature rules, and Smolyak sparse grid quadrature rules ([20]). A brief introduction to Smolyak sparse grid rules and some details about choice of quadrature rules are given in the Appendix 6.2. In Figure 1 we show examples of meshes with prescribed quadrature points for two-dimensional ($N = 2$) parameter space Γ.

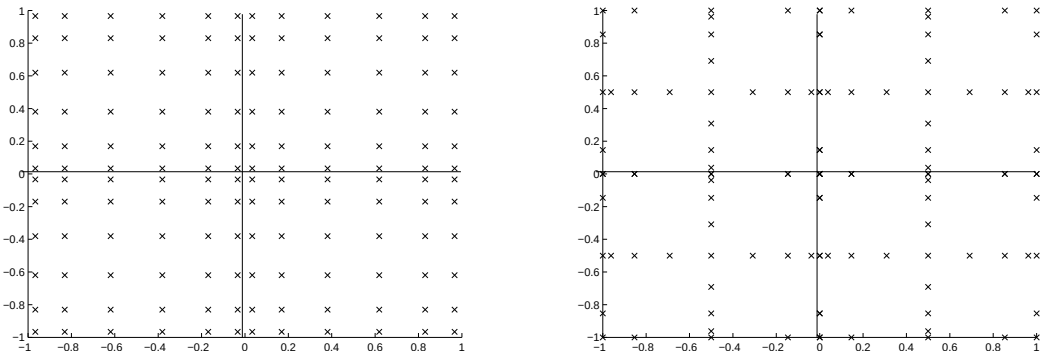

Figure 1: Left: Tensor-product Gauss-Legendre quadrature grid in $N = 2$ dimensions with a 4-element uniform mesh. Right: Clenshaw-Curtis Smolyak sparse quadrature grid in $N = 2$ dimensions with a 4-element uniform mesh. The solid lines denote the boundaries between elements.

2.0.2 Step 2: Characterize biological markers

The next step is to develop mathematical metrics, or markers, that characterize the biological outcomes of interest. These metrics can depend on the solution itself, $\boldsymbol{x}$, as well as temporal and spatial variables. The inherent generality of these metrics is one of the strengths of the ME-PCM since we can calculate the sensitivity of a large variety of biologically relevant quantities. Determining the sensitivity of these metrics to varying parameters is described in the third step of the ME-PCM procedure. Below we provide three example metrics that are relevant in most cellular signaling networks.

Metric 1 - System sensitivity. Here, we are interested in determining the overall sensitivity of the system to random initial conditions. In this case, we may define the sum of the variance of all molecular species concentrations to be a measure of system sensitivity in each element S_{B^i} at time t. Recall that the variance of a uniform random variable X on a (possibly multidimensional) interval I is the expected value of X^2 minus the squared expected value of X. Also recall that the expected value of a function $v(X)$ is given by:

$$\mathbb{E}[v(X)] = \frac{1}{\text{vol}(I)} \int_I v(y) dy$$

where the $\frac{1}{\text{vol}(I)}$ arises as the probability density function of X. Let $\text{vol}(B^i)$ denote the volume of the element B^i. Using the above formulation and the numerical integration rule set in (3),

we may now write an approximate expression for S_{B^i}:

$$\begin{aligned} S[B^i](t) \equiv \sum_{j=1}^{N} \mathrm{Var}_{B^i}\left[x_j(t,\boldsymbol{Y})\right] &= \sum_{j=1}^{N} \left(\mathbb{E}[x_j(t,\boldsymbol{Y})^2] - \mathbb{E}[x_j(t,\boldsymbol{Y})]^2\right) \\ &= \sum_{j=1}^{N} \left(\frac{1}{\mathrm{vol}(B^i)}\int_{B^i} x_j^2(t,\boldsymbol{y})d\boldsymbol{y} - \left(\frac{1}{\mathrm{vol}(B^i)}\int_{B^i} x_j(t,\boldsymbol{y})d\boldsymbol{y}\right)^2\right), \end{aligned} \tag{4}$$

where Var_{B^i} denotes the variance of a random quantity over B^i.

Since this metric sums over the variances of all N species, it reflects a measure total sensitivity of the system to parametric variation. Thus we expect the sensitivity results obtained using this metric to correspond loosely to those obtained using the DLE analysis in ([9]), although the mathematical definition of system sensitivity in these two methods is substantially different.

Metric 2 - Molecular species-specific sensitivity. We might also be interested in determining the sensitivity of individual protein concentrations in the system. To this end, the sensitivity of the concentration x_k in each element is defined as:

$$S[B^i, x_j](t) \equiv \mathrm{Var}_{B^i}\left[x_j(t,\boldsymbol{Y})\right] \equiv \frac{1}{\mathrm{vol}(B^i)}\int_{B^i} x_j^2(t,\boldsymbol{y})d\boldsymbol{y} - \left(\frac{1}{\mathrm{vol}(B^i)}\int_{B^i} x_j(t,\boldsymbol{y})d\boldsymbol{y}\right)^2. \tag{5}$$

This equation, similar to (4), defines the sensitivity as the variance of the random quantity $x_k(t,\boldsymbol{Y})$ over the element B^i. Likewise, analagous markers can be defined for all other proteins in the system.

Metric 3 - Total exposure of a single molecular species. The total exposure of the system to a particular molecular species may play an important role in system dynamics, especially in situations where irreversible decisions are made such as developmental or death/survival signals. Mathematically, this amounts to the integration of the concentration of the molecular species x_j in time. Denote this integrated quantity by $f(\boldsymbol{Y},t) = \int_0^t x_j(s,\boldsymbol{Y})ds$; since the concentration x_j is a quantity with random dependence through $\boldsymbol{Y}$, f also carries a random dependence. We can define a marker to study the sensitivity of this integrated value f to random initial conditions:

$$\begin{aligned} M[B^i, I(x_j)](t) &\equiv \mathbb{E}[f(\boldsymbol{Y},t)] = \frac{1}{\mathrm{vol}(B^i)}\int_{B^i} f(t,\boldsymbol{y})d\boldsymbol{y} \\ &= \frac{1}{\mathrm{vol}(B^i)}\int_{B^i}\int_0^t x_j(s,\boldsymbol{y})dsd\boldsymbol{y}. \end{aligned} \tag{6}$$

Metric 4 - General user-defined outputs. Using the ME-PCM, it is possible to analyse the sensitivity of many biological markers at once without additional sampling. The generality of these markers or metrics allows the user to define sensitivity in terms of biologically relevant quantities for each problem.

For example, higher moments such as variance, skewness and kurtosis of the integrated value used in Metric 3 could be defined as sensitivity measures. The 'skewness' or normalized centered third moment of the data effectively shows the propensity of a random quantity to be higher or lower than the mean value. In a region where the mean is near a threshold, a negative skewness would indicate a propensity to values above the mean. Figure 10 in the Appendix shows examples of probability distribution functions with positive and negative skewness.

2.0.3 Step 3: Sampling and postprocessing

The main computational effort in the ME-PCM lies in the sampling step, in which the solution of the problem (2) is computed with initial condition set to each quadrature point in each element. The set of initial conditions (or samples) is given as $\{\boldsymbol{q}_j^i\}$ for $i = 1...N_e$ and $j = 1...r$ where the $\boldsymbol{q}_j^i$ are prescribed by the quadrature rule in (3). Recall that r is the number of points in the quadrature rule and N_e is the number of elements in the mesh; thus there are rN_e sampling points in total. The discretization used to compute the solution at each sample point is up to the user; in this work we use MATLAB's ode15s to discretize (2) as in ([9]).

After sampling, we obtain a set of solutions: $\{\boldsymbol{x}(t, \boldsymbol{q}_j^i)\}$ for $i = 1...N_e$ and $j = 1...r$. We next postprocess the solutions to obtain approximations to the markers chosen in step 2. Using the numerical quadrature rules we have prescribed in each element, the moment integrals in the marker definitions are approximated by weighted summations.

Metric 1 - System sensitivity. For example, we approximate the integrals in (4) using the quadrature rule (3). Written explicitly, we have:

$$\begin{aligned} S[B^i](t) &= \sum_{j=1}^{N} \left(\frac{1}{\text{vol}(B^i)} \int_{B^i} x_j^2(t, \boldsymbol{y}) d\boldsymbol{y} - \left(\frac{1}{\text{vol}(B^i)} \int_{B^i} x_j(t, \boldsymbol{y}) d\boldsymbol{y} \right)^2 \right) \\ &\approx \sum_{j=1}^{N} \left(\frac{1}{\text{vol}(B^i)} \sum_{k=1}^{r} x_j^2(t, \boldsymbol{q}_k^i) w_k^i - \left(\frac{1}{\text{vol}(B^i)} \sum_{k=1}^{r} x_j(t, \boldsymbol{q}_k^i) w_k^i \right)^2 \right) \end{aligned} \tag{7}$$

where the integrals from the expected value have been approximated by numerical quadrature

sums, utilizing the set of solutions $\{\boldsymbol{x}(t, \boldsymbol{q}_j^i)\}$ at each quadrature point.

Metric 2 - Species-specific sensitivity. Similarly, the variance of casp-3* concentration in element B^i is approximated by:

$$S[B^i, x_j](t) \approx \frac{1}{\text{vol}(B^i)} \sum_{k=1}^{r} x_j^2(t, \boldsymbol{q}_k^i) w_k^i - \left(\frac{1}{\text{vol}(B^i)} \sum_{k=1}^{r} x_j(t, \boldsymbol{q}_k^i) w_k^i \right)^2 \tag{8}$$

where once again the integrals in (5) have been replaced by their respective numerical quadrature approximations.

Metric 3 - Total exposure of a single molecular species. Using the same technique we can approximate the mean of the total time-integrated amount of chemical x_j in element B^i:

$$M[B^i, I(x_j)](t) \approx \frac{1}{\text{vol}(B^i)} \sum_{k=1}^{r} \left(\int_0^t x_j(s, \boldsymbol{q}_k^i) ds \right) w_k^i \tag{9}$$

Here, note that the integral $\int_0^t x_j(s, \boldsymbol{q}_k^i)) ds$ is required. This is easily achieved by using a numerical integration in time, such as a trapezoid rule and storing the integrated quantity at each time step in addition to the solutions $x_j(s, \boldsymbol{q}_k^i))$.

3 Results

We demonstrate the ability of the ME-PCM to study various sensitivity measures of a biochemical system using some example metrics from the previous section. As a model problem, we use the apoptosis regulatory network model from ([9]). The network modeled is a key sub-network that regulates the decision for a cell to live or die. The apoptosis network has been studied previously as a system where survival and death are each a stable locally attracting steady-state ([21, 22]). However, other work suggests that the decision for cell apoptosis is determined by a transient response. That is, in response to external stimuli this sub-network creates a transient response that signals cell survival or cell death ([9, 21]).

We first introduce the model of the apoptosis regulatory network and demonstrate the same region of sensitivity determined in ([9]). We then go on to study this region in greater detail with the metrics developed in section 2. Using the ME-PCM we study the emergence of the region of sensitivity as a function of time and variation in individual molecular species. In doing so, we demonstrate that the system is most sensitive to perturbations in activated caspase 8. In addition, we use integrated values and skewness (metrics 3 and 4 from section 2) to investigate the fate of cells within the highly sensitive region. Finally, we consider the sensitivity of the system to varying initial conditions and reaction rates.

3.1 Model Problem: Apoptosis Regulatory Network

A system of 8 ordinary differential equations models the caspase activation cascade (see (10) and Tables 1 and 2). This model considers the apoptosis signaling network as having two pathways: survival and death (see Figure 1 from [9]).

The pathway to cell death consists of caspase activation. The cascade begins with activation of the initiator caspase, caspase-8, which then activates the effector caspase, caspase-3. (The caspases are created in the in-active state. In Figure 1 from ([9]) the superscript $*$ indicates activation.) Apoptosis is effected by active caspase-3, which cleaves hundreds of protein substrates, thus killing the cells. XIAP, X-linked inhibitor of apoptsosis, negatively regulates the activity of casp-3* by tagging casp-3 for ubiquitination; this action promotes the dissassociation of casp-3 and reduces its activity. As discussed in [9], this model is mechanistic in nature and does not explicitly model every protein in the apoptosis signaling network. However, this model does capture the signal for cell death coming in the form of a transient response.

$$
\begin{aligned}
\dot{x_1} &= -k_1 x_4 x_1 + k_{d1} x_5 \\
\dot{x_2} &= k_{d2} x_5 - k_3 x_2 x_3 + k_{d3} x_6 + k_{d4} x_6 \\
\dot{x_3} &= -k_3 x_2 x_3 + k_{d3} x_6 \\
\dot{x_4} &= k_{d4} x_6 - k_1 x_4 x_1 + k_{d1} x_5 - k_5 x_7 x_4 + k_{d5} x_8 + k_{d2} x_5 \\
\dot{x_5} &= -k_{d2} x_5 + k_1 x_4 x_1 - k_{d1} x_5 \\
\dot{x_6} &= -k_{d4} x_6 + k_3 x_2 x_3 - k_{d3} x_6 \\
\dot{x_7} &= -k_5 x_7 x_4 + k_{d5} x_8 + k_{d6} x_8 \\
\dot{x_8} &= k_5 x_7 x_4 - k_{d5} x_8 + k_{d6} x_8
\end{aligned}
\tag{10}
$$

Table 1: Key for chemical compounds in equations (10). (*) denotes activation, :ub denotes ubiquitination tag

symbol	molecular species	initial concentration range
x_1	casp-8	10^2 to $3.5(10)^5$ mol/cell
x_2	casp-8*	10^2 to 10^5 mol/cell
x_3	casp-3	10^2 to $3.5(10)^5$ mol/cell
x_4	casp-3*	10^2 to 10^5 mol/cell
x_5	casp-8:casp-3*	10^2 to $2.5(10)^4$ mol/cell
x_6	casp-8*:casp-3	10^2 to $2.5(10)^4$ mol/cell
x_7	XIAP	10^2 to 10^5 mol/cell
x_8	casp-3*:XIAP	10^2 to $2.5(10)^4$ mol/cell

3.2 Sensitivity to Initial Conditions

3.2.1 Metric 1: System sensitivity

We first study the sensitivity of the system to varying initial concentrations at the time $t = 6$ hours. In the discussion in ([9]), the time of 6 hours is identified as a time by which all of their cell lines would have responded to treatment designed to induce cell death. As in ([9]), we model the initial conditions as uniformly distributed in the ranges given in Table 1. Thus, our random dimension is 8.

Table 2: Key for reaction rates in equations (10). These values are used for the rate constants throughout unless otherwise noted.

symbol	rate constants	value
k_1	binding rate of casp-8,casp-3*	$2.67(10)^{-9}$cell*(s*mol)$^{-1}$
k_3	binding rate of casp-8*, casp-3	$6.8(10)^{-8}$cell*(s*mol)$^{-1}$
k_5	binding rate of casp-3*, XIAP	$7(10)^{-5}$cell*(s*mol)$^{-1}$
k_{d1}	dissociation rate of x_5 to casp-8, casp-3*	$1(10)^{-2}$s^{-1}
k_{d2}	dissociation rate of x_5 to casp-8*, casp-3*	$8(10)^{-3}$s^{-1}
k_{d3}	dissociation rate of x_6 to casp-8*, casp-3	$5(10)^{-2}$s^{-1}
k_{d4}	dissociation rate of x_6 to casp-8*, casp-3*	$1(10)^{-3}$s^{-1}
k_{d5}	dissociation rate of x_8 to XIAP, casp-3*	$1.67(10)^{-5}$s^{-1}
k_{d6}	dissociation rate of x_8 to XIAP, casp-3*:ub	$1.67(10)^{-4}$s^{-1}

We discretize the parameter space with 10 elements in the casp-8* and XIAP ranges each, 9 elements in each of the remaining caspase ranges, and 1 element in each of the chemical intermediate ranges. The ME-PCM is performed using 100 elements in a uniform mesh and a sparse Clenshaw-Curtis grid of 317 points per element.

In this and following examples, we plot the results on a two-dimensional slice of elements in the parameter mesh. Specifically, the results are plotted on all elements in the XIAP-casp-8* plane containing the following initial conditions: $2.6(10)^5$ mol/cell of casp-3, 100 mol/cell of casp-3* and intermediate complexes), and $1.7(10)^5$ mol/cell of casp-8. Figure 2 shows the results of this case in the XIAP-casp-8* plane at a time of 6 hours. The grid of circles represents the mesh used in the problem, and the colour of each circle represents the value of the sum of species variances as defined in Metric 1. A large region of high system sensitivity is observed in the XIAP-casp-8* plane. It remains relatively constant throughout the initial condition range of casp-8. This region agrees with the described separatrix in ([9]) that is thought to delineate the regimes of cell death and survival. However, it is important to note that the high-sensitivity regions found using the ME-PCM are mathematically different from separatrices. These high-sensitivity regions indicate locations in parameter space where perturbations to initial conditions cause large variation in system behavior; thus they do not necessarily 'separate' the parameter space in every problem.

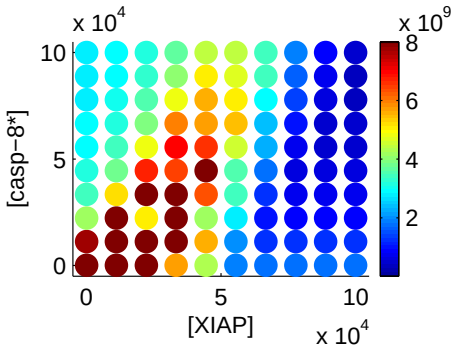

Figure 2: System sensitivity, $S[B^i](t)$, at $t = 6$ hours in casp-8*-XIAP plane for the case of all initial conditions random. The horizontal axis represents the initial concentration of XIAP and the vertical axis represents the initial concentration of casp-8* in mol/cell. Warm colours indicate high sensitivity, cooler colours indicate low sensitivity. Region of high sensitivity agrees with DLE separatrix found in ([9]) separating the survival and death regions of the parameter space.

3.2.2 Metric 1: Time-varying system sensitivity

Without performing any additional samples of the system, we are able to also output the following sensitivity analyses via additional postprocessing (weighted summations). Figure 3 shows snapshots of the system sensitivity at various points in time. By generating a system sensitivity map at various time increments, we are able to study the evolution of the sensitivity maps in time. The same input parameters are used as in the previous section, and the results are visualized in the same XIAP-casp-8* plane. In these plots, the variance is normalized by its maximum value over the parameter space and time so that the same colourscale between 0 and 1 may be used throughout the time series. These kinds of maps can provide a useful tool in deciding parameter regimes for more detailed experimental testing. For example, in this model problem, performing experiments in the initial-concentration regime within the high-sensitivity region could lend much more insight into the mechanism of the cell decision than experimental investigation of other regions of the parameter space.

Time-varying sensitivity maps can provide useful information about the time scale of system dynamics within the course of an experiment. In this case, we see that the high sensitivity region we observe in Figure 2 is actually formed and stabilized by time $t = 3$ hours, suggesting that the cell decision is made by that time. Also, we note the high sensitivity of the system at early times. This suggests that if the system is perturbed experimentally during this stage the outcome is more easily changed than by intervention at a later stage.

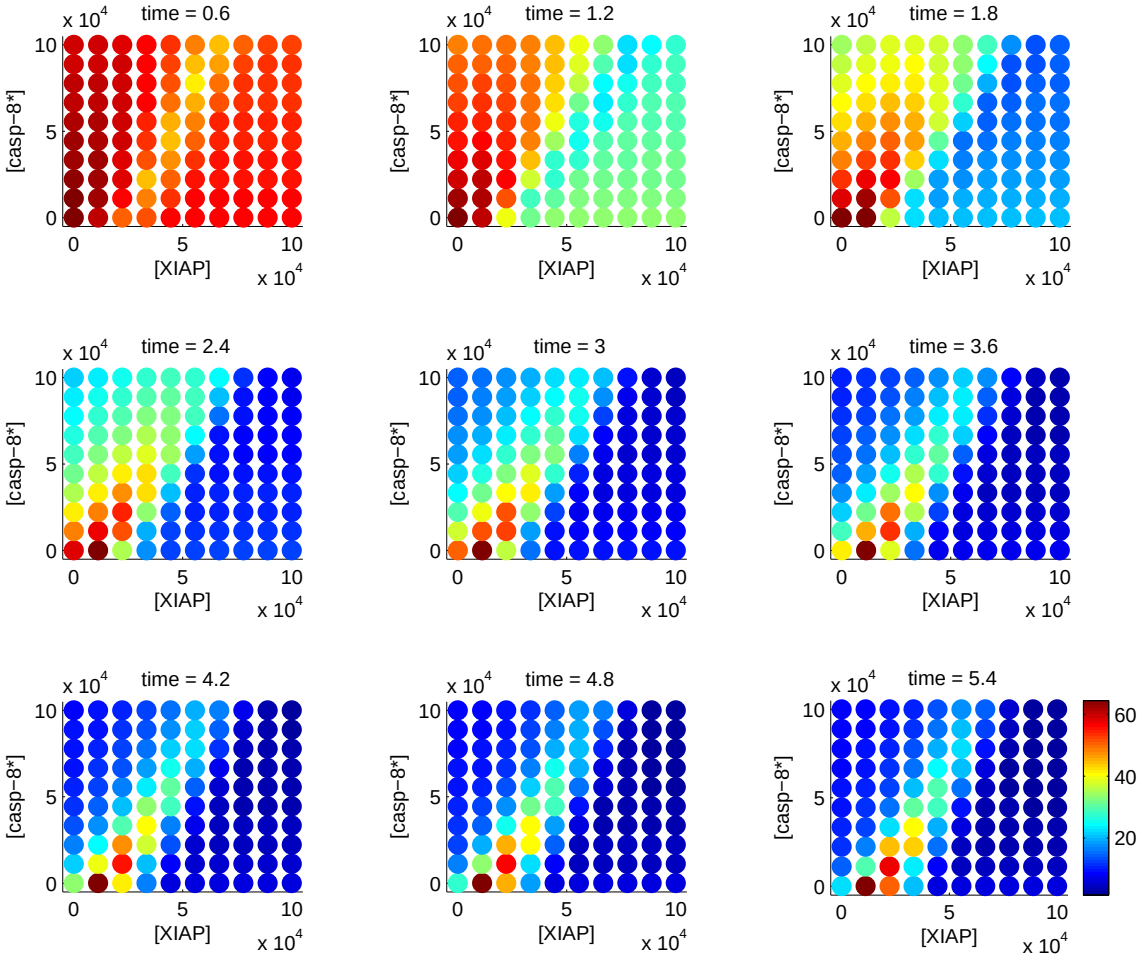

Figure 3: We plot the system sensitivity to varying initial conditions, $S_{B^i}(t)$, in each element at various snapshots in time from $t = 0$ to $t = 6$ hours. The horizontal axis represents the initial concentration of XIAP and the vertical axis represents the initial concentration of casp-8* in mol/cell. The colourscale is conserved across the series, with the variance normalized by its maximum value over the parameter space and time. The snapshots demonstrate the emergence/evolution of the separatrix in time. Note that there is little change in the regions of high sensitivity between $t = 3$ and $t = 6$; this indicates potentially at what time the cellular response is determined.

3.2.3 Metric 2: Molecular species-specific sensitivity

We may also be interested in studying the sensitivity of specific components of the system. Using the marker formulated in Metric 2, we plot the sensitivity of the activated effector caspase (casp-3*), $S[B^i, x_4](t)$, as a function of time in Figure 4. We note that the high sensitivity regions in

the lower left corner eventually fade away. This is evidence of the transient nature of the signal; all trajectories of casp-3* eventually reach a steady state at zero concentration and the system thus becomes insensitive to parameter changes at later times.

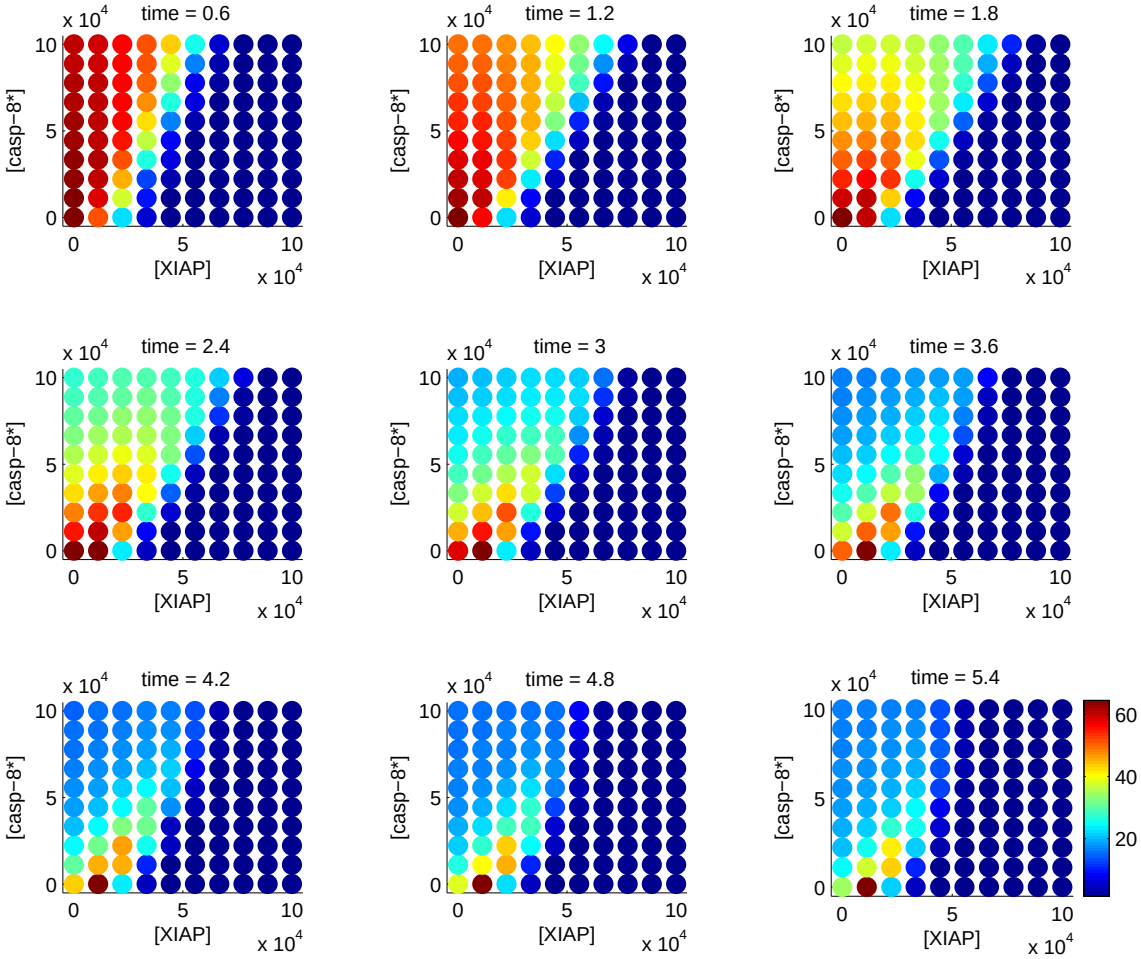

Figure 4: Maps of casp-3* sensitivity, $S[B^i, x_4](t)$, at various times until $t = 6$ hours. The horizontal axis represents the initial concentration of XIAP and the vertical axis represents the initial concentration of casp-8* in mol/cell. As mentioned previously, snapshots are taken ar regular intervals and the colourscale is conserved across the series, with the variance normalized by its maximum value over the parameter space and time.

Figure 5 shows analagous sensitivity maps for the activated caspase-8. Here we note that the system sensitivity is largely dominated by the sensitivity of casp-8*, since a similar high

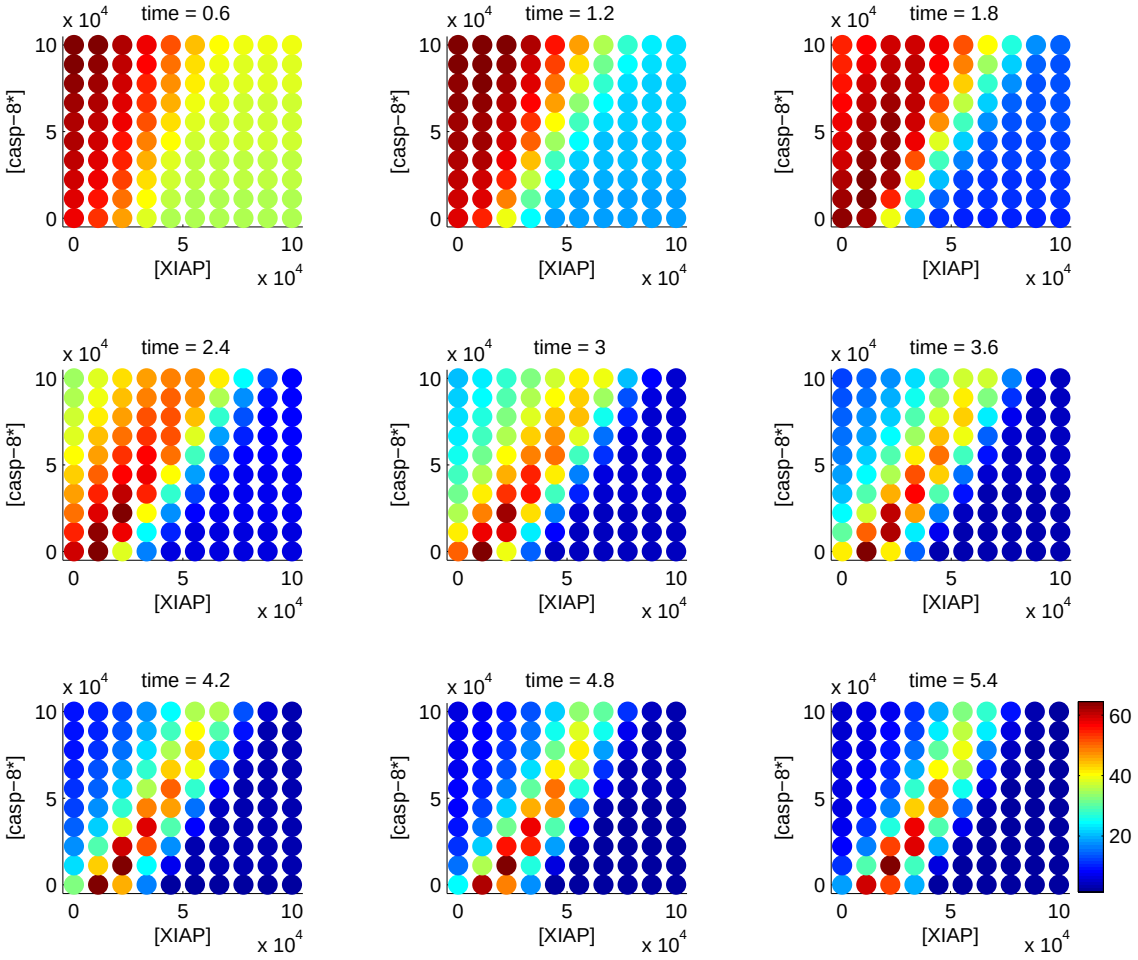

Figure 5: Maps of casp-8* sensitivity, $S[B^i, x_2](t)$, at various times until $t = 6$ hours. In each plot, the horizontal axis represents the initial concentration of XIAP and the vertical axis represents the initial concentration of casp-8* in mol/cell. Snapshots are taken ar regular intervals and the colourscale is conserved across the series, with the variance normalized by its maximum value over the parameter space and time. Note that the high sensitivity region is stable after $t = 3$ and closely corresponds to the region of high global system sensitivity in figure 2, suggesting that the sensitivity of this species provides a large contribution to the global system sensitivity.

sensitivity region appears in these plots. This indicates that the system will be most sensitive to perturbations in casp-8*, and this insight can be useful in motivating experimental design.

3.2.4 Metric 3: Integrated casp-3*

We now focus our attention on Metric 3, which marks the total exposure to activated caspase-3 over time. The horizontal axis represents the initial concentration of XIAP and the vertical axis represents the initial concentration of casp-8* in mol/cell. Since the cell decision is made based on prolonged activation of caspase-3, we hypothesize that the total exposure (i.e., integrated value) of activated caspase-3 is important to the outcome. Figure 6 shows the mean value of the integrated casp-3* at time $t = 6$ hours. Note that the integrated value increases monotonically for decreasing XIAP initical conditions. This is somewhat intuitive since the pro-survival XIAP tags casp-3* for ubiquitination. In addition, the region of sensitivity seems to be consistent with the total exposure to casp-3*.

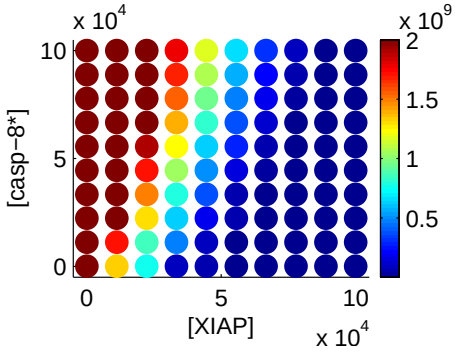

Figure 6: Mean of integrated casp-3* concentration, $M[B^i, I(x_4)](t)$, at $t = 6$ hours for the same variable initial conditions as used in all previous examples. The sensitivity marker is defined to be the mean value of the total (integrated) amount of activated caspase-3 present in the cell until $t = 6$ hours.

3.2.5 Metric 4: Skewness of the integrated casp3* value

Thus far we have identified the same region of sensitivity as observed in [9] separating cell survival from cell death. However, it remains to be demonstrated what tendency, if any, cells within the separatrix may have towards survival or death. The generality of the ME-PCM allows us to interrogate the fate of cells within the region of uncertainty. As an indication of the propensity of cell death, we study the skewness of the integrated casp-3* concentration in our system.

As figure 6 shows, the total exposure of a cell to caspase-3* varies continuously from lowest values in the survival region to highest values in the death region, with cells in the separatrix

having intermediate levels of exposure.

As previously mentioned, skewness indicates the propensity of a distribution to be above or below the mean (see Figure 10 in the appendix). Figure 7 shows the skewness of integrated casp-3* at $t = 6$ hours (values have been normalized). Most of the cells in the survival and death regions of the space have skewness close to 0, indicating the integrated casp-3* concentrations are fairly symmetrically distributed in these regions of space. However, the skewness is positive within the separatrix indicating that the casp-3* distribution has a tendency to be less than the mean. The positive skew suggests that cells within separatrix have a tendency towards lower (i.e., potentially survival) levels of integrated casp-3*.

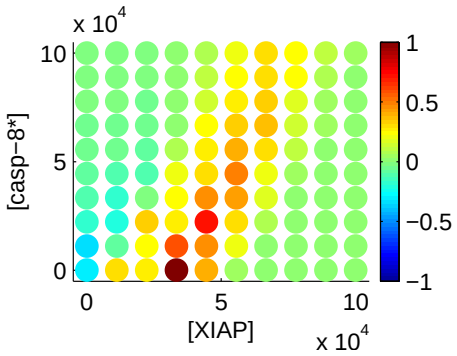

Figure 7: Skewness of integrated casp-3* concentration at $t = 6$ hours for the same variable initial conditions as used in all previous examples. The horizontal axis represents the initial concentration of XIAP and the vertical axis represents the initial concentration of casp-8* in mol/cell. The sensitivity values have been normalized to scale between -1 and 1. Negative values indicate that the integrated value is more likely to fall above the mean, and positive values indicate that the integrated value is more likely to fall below the mean. The zero-skewness neutral colour (green) indicates that the distribution places equal mass above and below the mean.

3.3 Sensitivity to varying initial conditions and reaction rates

In the next section we aim to study the sensitivity of the system to varying reaction rates in addition to initial conditions. The initial conditions are taken to be uniformly distributed over the ranges given in Table 1, and as in ([9]) we investigate sensitivity of the system to varying the ubiquitination rate k_{d6}. More generally we allow k_{d6} to vary between $1.7(10)^{-5}$ and $6.17(10)^{-4}$.

In Figure 8 we show the system sensitivity results on the XIAP-casp-8* slice and at time $t = 6$ hours. Here, a 600-element mesh is used to discretize the 9-dimensionsal random space, with a 181-point sparse Clenshaw Curtis grid in each element. Six equally-sized elements are

used to discretize the k_{d6} direction, and the results are plotted separately for each of these elements. We observe that the location and shape of the high-sensitivity region is very sensitive to the ubiquitination rate, especially in the lower regime. As the rate is lowered, the sensitive region shifts to locations of high XIAP-low casp-8* initial conditions and the region of likely cell death is enlarged. As the rate increases, the sensitive region shifts to the lower initial values of XIAP, and cell survival is expected in most of the parametric domain.

Next we consider the effect of uncertain k_{d2}, which is the degradation rate of x_5 to casp-8*, casp-3* in addition to uncertain initial conditions. Simulation parameters are the same as in the previous example, and in Figure 9 we plot here the results for 4 elements in the k_{d2} discretization. We observe that the shape and location of the region of high sensitivity is fairly robust to variations in k_{d2}.

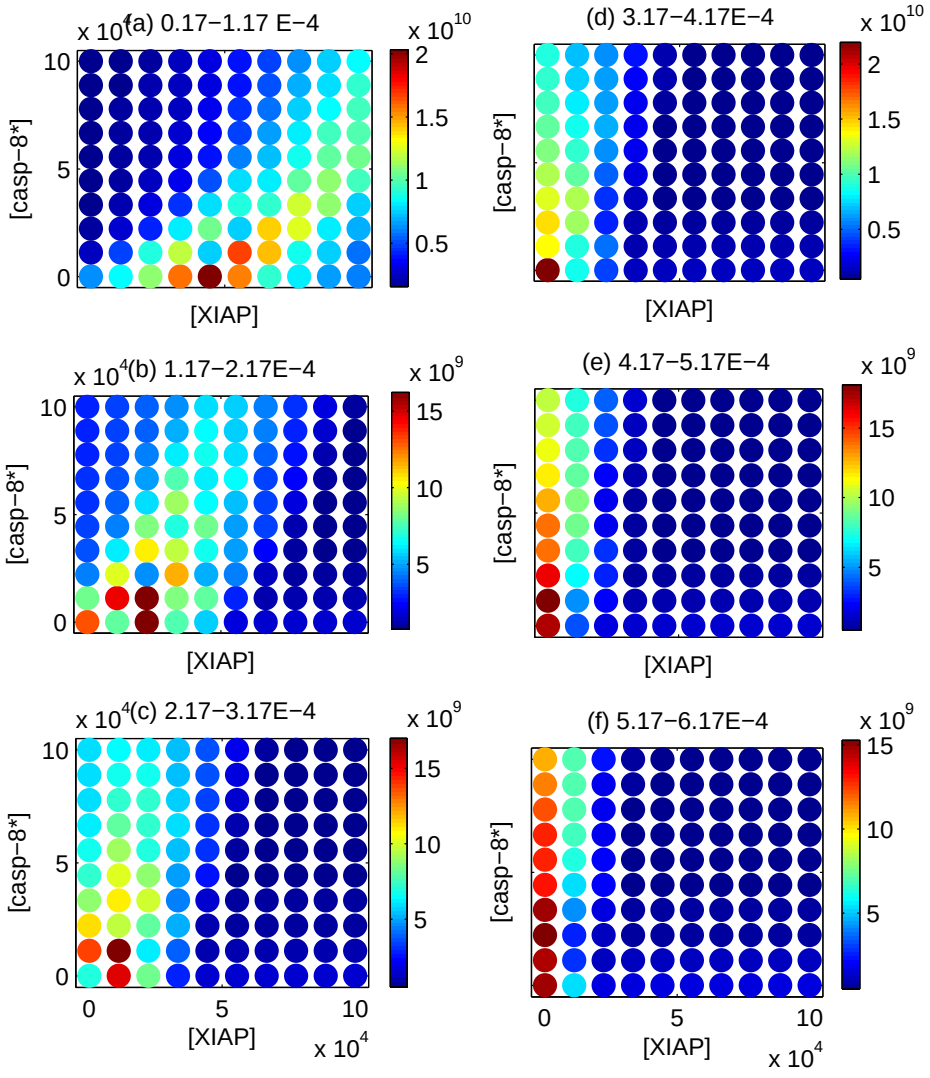

Figure 8: System sensitivity, $S[B^i](t)$, at $t = 6$ hours on XIAP-casp-8* plane for the case where the ubiquitination rate k_{d6} and the initial conditions are taken to be uniformly varying random variables. The horizontal axis represents the initial concentration of XIAP and the vertical axis represents the initial concentration of casp-8* in mol/cell. Results are plotted on the same XIAP-casp-8* plane as in other graphs, for each element in the k_{d6} mesh discretization. The ubiquitination rate constant k_{d6} varies over (a) $1.7(10)^{-5}$ to $1.17(10)^{-4}$; (b) $1.17(10)^{-4}$ to $2.17(10)^{-4}$; (c) $2.17(10)^{-4}$ to $3.17(10)^{-4}$; (d) $3.17(10)^{-4}$ to $4.17(10)^{-4}$; (e) $4.17(10)^{-4}$ to $5.17(10)^{-4}$; (f) $5.17(10)^{-4}$ to $6.17(10)^{-4}$.

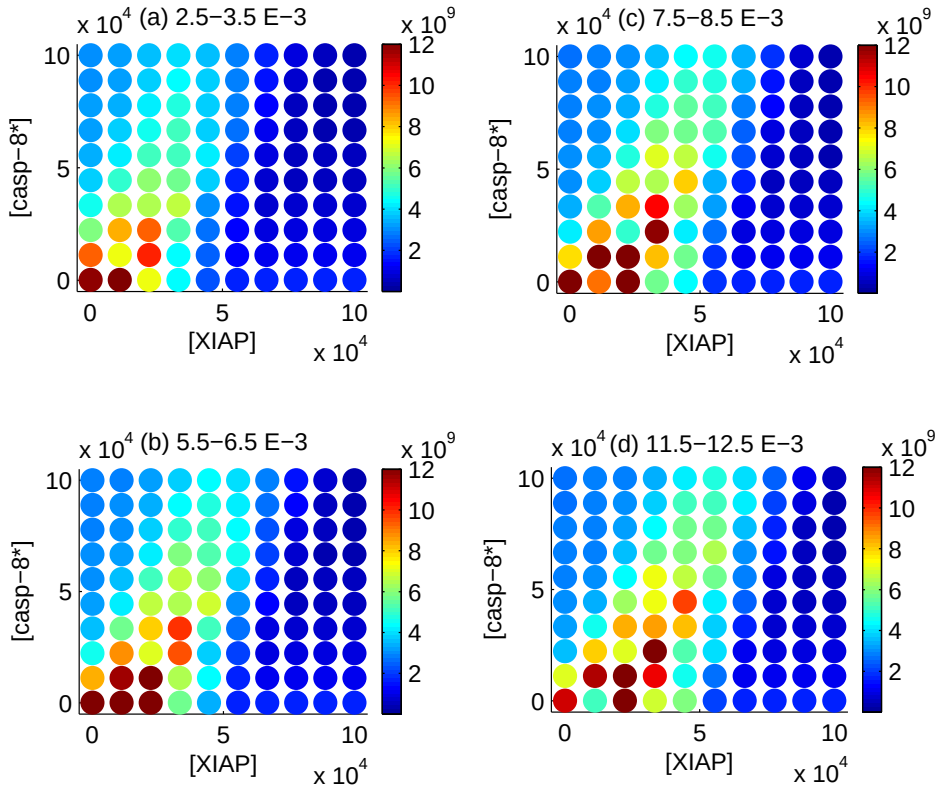

Figure 9: System sensitivity, $S[B^i](t)$, at $t = 6$ hours on XIAP-casp-8* plane for the case where k_{d2} and all initial conditions are taken to be uniformly varying random variables. The horizontal axis represents the initial concentration of XIAP and the vertical axis represents the initial concentration of casp-8* in mol/cell. The rate k_{d2} varies over the ranges (a) 0.0025 to 0.0035; (b) 0.0055 to 0.0065; (c) 0.0075 to 0.0085; (d) 0.0115 to 0.0125.

4 Discussion

We have described a general method suitable for analysis of any large dimensional ODE or PDE, but is particularly useful for biological signaling networks. In this section we discuss in more detail the benefits of our approach. In particular, we describe how incorporating adaptivity can greatly increase the computational efficiency of our method. In addition, we contrast our method with gradient-based methods, such as those in ([9]).

Applications of the ME-PCM. We have described how the ME-PCM can be used to study system sensitivity in biological systems. This type of information can be used to aid in experimental design and data analysis. The time-varying version of the ME-PCM can be used, for example, to predict the time at which a system should be perturbed in order to modify the outcome. It could also be used to estimate the time at which measurements of the system should be made (if a separatrix has already emerged). In general, we expect that ME-PCM sensitivity analysis results can be helpful in validating or invalidating models, and to aid in the construction of better models.

Generality of ME-PCM Analysis. The most attractive feature of the ME-PCM is its ability to study the sensitivity of general, user-defined, biologically relevant features of the system. The ME-PCM provides the user with the flexibility to study the sensitivity of any quantity that can be mathematically obtained using any components of the system solution at a current or previous time.

In our example problem, the apoptosis regulatory network, the biological outcome was most affected by perturbations in only a few components. By analyzing a variety of metrics we were able to determine which ones were most important.

Connection to Gradient-Based Methods. It is important to address the connections and differences between the variance-based approach that we propose and the more standard gradient-based techniques currently in use in systems biology. We begin by noting an intuitive connection between these two perspectives; in the Appendix (section 6.3) we demonstrate that as the size of ME-PCM elements goes to zero, the variance over the element converges to the square of the gradient, normalized by a factor. Thus, gradient-based methods essentially represent a limiting case of the ME-PCM. Both methods will identify regions of high sensitivity

indeed, as demonstrated in our results sections for the apoptosis model.

In addition to the flexibility of output mentioned previously, there is a key philosophical difference between these two approaches. In computing the variance over an element, we evaluate the sensitivity of the output caused by noisy parameters varying over a particular parameter range of a finite size h. This value of h directly affects the magnitude of the sensitivity output; by sampling points within each element we are able to compare the noise level and range of parameter inputs to the noise level and range of the outputs.

On the other hand, the local nature of the gradient calculation provides us only with approximated derivative information at each sampling point. In taking this gradient calculation as a measure of sensitivity at a point (and within a small range around that point), one must be confident in the precision of the model. Typically, mathematical models used in biology involve simplifications at physical scales. By looking at an exact gradient of the system at a point, our results could be very sensitive to small structural changes in the model.

Therefore, being able to compare the noise level and range of inputs to the noise level and range of the outputs will aid in the design and analysis of these imperfect models. Evaluating local variances may give a more robust representation of sensitivity for biological applications because, in a sense, computing variance assumes that the model is only locally reasonable and not locally correct. For this reason, we feel that a variance-based approach such as the ME-PCM provides a novel perspective to this problem that is not currently offered by gradient-based methods.

Computational considerations. The ME-PCM hails from the class of stochastic spectral methods, which comprise an emerging field of computationally efficient, highly accurate moment estimation techniques. Along with all other members of this class of methods, ME-PCM has been shown to reduce computation time by several orders of magnitude as compared to Monte Carlo methods when the random dimension is moderate ($N < 50$) ([13, 23, 24]). In addition, the sensitivities of multiple user-defined metrics at any time t can all be computed during postprocessing without additional sampling.

The ME-PCM also provides a few computational advantages over gradient-based methods. Specifically, a numerical gradient requires information from both sides of the point in question, so boundary errors may exist at any edge of the parameter space. Depending on the coarseness of the sampling grid, these boundary effects may creep several grid points into the domain and

become very large at corners of the parameter space. In contrast, the ME-PCM suffers from no such boundary effects, since no gradients are evaluated. Also, in moderately high dimensions the post-sampling costs of computing the gradient matrix are quite expensive, requiring finite differences for in each dimension for every point. In contrast, the variance calculation requires only a simple weighted summation.

Another computational benefit of the ME-PCM is the ability to resolve discontinuities or irregularity in the dependence of a sensitivity metric on the parameters. Elemental decomposition of the parameter space allows us to finely resolve around discontinuities in the sensitivity, so that the numerical quadrature remains accurate. This is particularly useful in biological threshold phenomenon, wherein an outcome may drastically change after a parameter is increased or decreased past a certain threshold. If the location or existence of such discontinuities is unknown beforehand, an adaptive version of the ME-PCM may be employed.

An adaptive version of the ME-PCM has been developed in ([13]) based on the adaptivity criterion designed in ([25]) which utilizes a generalized Polynomial Chaos basis (gPC). In this method, the size of the elements B^i are adaptively chosen so that large elements are used in regions where the solution is relatively smooth, and small elements are used when more refinement is needed. This type of adaptivity requires a robust "splitting" criterion for deciding where more refinement is needed. The splitting criterion in ([25]) involves projecting the solution within each element onto a gPC basis and analyzing the fractional contribution of the highest basis modes to the total variance in the element. In ([13]), this adaptive version of the ME-PCM was demonstrated to be highly efficient at locating discontinuities and adaptively resolving the mesh around them. In addition, this adaptive version was shown to be far more computationally efficient than other existing techniques with similar capability. Adaptivity greatly enhances the efficiency of the computations by reducing computational effort in smooth sections of the domain and should thus be used in systems with a large number of parameters and/or discontinuities in solution sensitivity. For the model apoptosis regulatory network, this was not needed since the dimension of the problem N was quite small and the system varies smoothly with parameter changes.

5 Acknowledgements

The authors would like to thank Dr. Bree Aldridge and Professor Doug Lauffenburger at MIT for their helpful discussion. In addition, the authors would like to acknowledge the support of DOE grant number DE-FG02-07ER25818. J. Foo would like to acknowledge the support of the DOE Computational Science Graduate Fellowship under grant number DE-FG02-97ER25308 and the Krell Institute.

References

[1] Riel N. Dynamic modelling and analysis of biochemical networks: mechanism-based models and model-based experiments. Briefings in Bioinformatics. 2006;7:364–374.

[2] Ihekwaba AEC, Broomhead DS, Grimley RL, et al. Sensitivity analysis of parameters controlling oscillatory signalling in the NF-κB pathway: the roles of IKK and IκBα. IEE Proc Systems Biology. 2004;1:93–103.

[3] Schoeberl B, et al. Computational modeling of the dynamics of the MAP kinase cascade activated by surface and internalized EGF receptors. Nature Biotech. 2002;20:370–375.

[4] Gutenkunst RN, Waterfall JJ, Casey FP, Brown KS, Myers CR, et al. Universally Sloppy Parameter Sensitivities in Systems Biology Models. PLoS Computational Biology. 2007;3.

[5] Kholodenko BN, Demin OV, Westerhoff HV. Control Analysis of Periodic Phenomena in Biological Systems. J Phys Chem. 1997;101:2070–2081.

[6] van Stiphout RGPM, Verhoog PJ, van Riel NAW, et al. Computational model of excitable cell indicates ATP free energy dynamics in response to calcium oscillations are undampened by cytosolic ATP buffers. IEE Proceedings of Systems Biology. 2006;153:405–408.

[7] Wilkins AK, Barton PI, Tidor B. The Per2 Negative Feedback Loop Sets the Period in the Mammalian Circadian Clock Mechanism. PLoS Computational Biology. 2007;3.

[8] Ingalls B, Sauro H. Sensitivity analysis of stoichiometric networks: an extension of metabolic control analysis to non-steady state trajectories. J Theor Biol. 2003;222:23–36.

[9] Aldridge BB, Haller G, Sorger PK, Lauffenburger DA. Direct Lyapunov exponent analysis enables parametric study of transient signalling governing cell behaviour. IEE Proceedings of Systems Biology. 2006;153:425–432.

[10] Cho KH, Shin SY, Kolch W, Wolkenhauer O. Experimental design in systems biology, based on parameter sensitivity analysis using a Monte Carlo method: a case study for the TNFα-mediated NF-κB signal transduction pathway. Simulation. 2003;79:726–639.

[11] Zi Z, Cho KH, Sung MH, Xia X, Zheng J, Sun Z. In silico identification of the key components and steps in IFN-γ induced JAK-STAT signaling pathway. FEBS Lett. 2005;570:1101–1108.

[12] Cho K, Shin S, Kolch W, et al. Experimental design in systems biology, based on parameter sensitivity analysis using a Monte-Carlo method: a case study for the TNKα- mediated NF-κB signal transduction pathway. Simulation. 2003;79:729–739.

[13] Foo J, Wan X, Karniadakis G. The Multi-Element Probabilistic Collocation Method: Error Analysis and Applications. J Comp Physics. 2008;227:9572–9595.

[14] Ghanem RG. Ingredients for a general purpose stochastic finite element formulation. Comput Methods Appl Mech Engrg. 1999;168:19–34.

[15] Ghanem RG. Stochastic finite elements for heterogeneous media with multiple random non-Gaussian properties. ASCE J Engrg Mech. 1999;125(1):26–40.

[16] Matthies HG, Bucker CG. Finite Element for stochastic media problems. Comput Methods Appl Mech Engrg. 1999;168:3–17.

[17] Foo J, Yosibash Z, Karniadakis G. Stochastic Simulation of Riser-Sections with Uncertain Measured-Pressure Loads and/or Uncertain Material Properties. Comput Methods Appl Mech Engrg. 2007;196:4250–4271.

[18] Kim D, Debusschere BJ, Najm HN. Spectral Methods for Parametric Sensitivity in Stochastic Dynamical Systems. Biophys Journal. 2007;92:379–393.

[19] Tatang M, McRae G. Direct Treatment of Uncertainty in Models of Reaction and Transport. MIT Technical Reports. 1994;.

[20] Smolyak S. Quadrature and interpolation formulas for tensor products of certain classes of functions. Soviet Math Dokl. 1963;4:240–243.

[21] Eissing T, et al. Bistability analyses of a caspase activation model for receptor-induced apoptosis. J Biol Chem. 2004;279:36892–7.

[22] Bagci EZ, et al. Bistability in Apoptosis: Roles of Bax, Bcl-2 and Mitochondrial Permeability Transition Pores. Biophys J. 2005;.

[23] Ghanem RG, Spanos P. Stochastic Finite Elements: A Spectral Approach. Springer-Verlag, New York; 1991.

[24] Xiu D, Hesthaven J. High-Order Collocation Methods for Differential Equations with Random Inputs. SIAM J Sci Comput. 2005;27(3):1118–1139.

[25] Wan X, Karniadakis GE. An adaptive multi-element generalized polynomial chaos method for stochastic differential equations. J Comput Phys. 2005;209(2):617–642.

[26] Kincaid D, Cheney W. Numerical Analysis. Pacific Grove, CA, USA: Brooks/Cole Publishing Company; 1991.

[27] Barthelmann V, Novak E, Ritter K. High dimensional polynomial interpolation on sparse grids. Adv Comput Math. 2000;12:273–288.

[28] Novak E, Ritter K. High dimensional integration of smooth functions over cubes. Numer Math. 1996;75:79–97.

[29] Novak E, Ritter K. Simple cubature formulas with high polynomial exactness. Constr Approx. 1999;15:499–522.

6 Appendix

6.1 Example of skewness

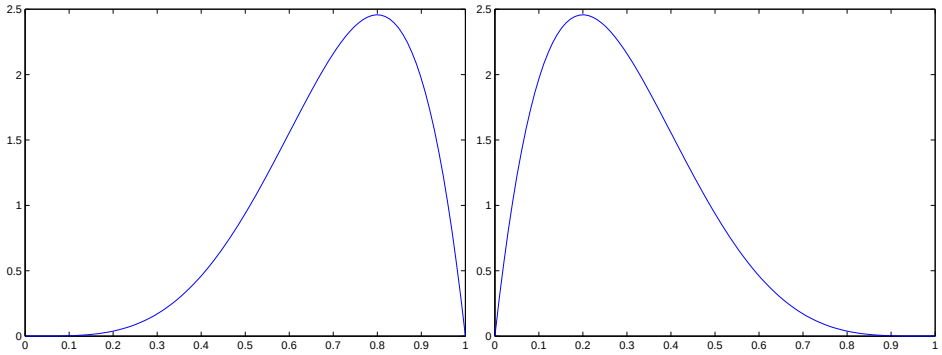

Figure 10: Left: A probability distribution (Beta(2,5)) function with negative skewness. Right: A probability distribution (Beta(5,2)) function with positive skewness.

6.2 Quadrature rules

We consider two main types of multi-dimensional numerical integration rules: tensor-product Gaussian quadrature rules, and Smolyak sparse grid quadrature rules. Gaussian quadrature rules are fairly well-known (see [26] for example) and provide high order accuracy (i.e. the class of functions for which equality holds in (3) is large). However, the computational complexity of tensorized Gaussian quadrature rules grows exponentially with increasing dimension N.

Smolyak sparse grids were introduced in ([20]) and provide an attractive alternative quadrature choice which scales favorably with increasing dimension. The following description of the Smolyak method closely follows the descriptions in ([27, 28] and [29]) where the interpolation and cubature errors and costs of this method are investigated.

We assume for simplicity that the parameter space $\Gamma = [-1, 1]^N$ without loss of generality, since the N-dimensional element can always be mapped to this standard element. We begin by choosing a one-dimensional quadrature formula $\mathcal{U}_j^i$ suited to the setting in which we are interested. More specifically, for functions $v : [-1, 1] \to \mathbb{R}$, choose a quadrature rule

$$\mathcal{U}_j^i(v) = \sum_{m=1}^{n_i} v(y_m^i) \cdot w_m^i$$

which approximates the integral

$$\int_{[-1,1]} v(y)dy$$

for $i \in \mathbb{N}$ and $j = 1, ..., N$. Here $i \in \mathbb{N}$ specifies the degree of the quadrature, n_i is the number of points used, the $\{y_m^i\}_{m=1}^{n_i}$ are quadrature points and the $\{w_m^i\}_{m=1}^{n_i}$ are quadrature wieghts. The index j indicates that this quadrature formula is used in the j-th dimension. In practice, we will always use the same formulas in every dimension, but for now we will retain the subscript in order to better elucidate the Smolyak construction.

This one-dimensional formula $\mathcal{U}_j^i$ could be chosen to be the a Gauss-Legendre quadrature rule, where the $\{y_m^i\}_{m=1}^{n_i}$ are the roots of the $(n_i - 1)$-th degree Legendre polynomials in the j-th dimension as described above and the $\{w_m^i\}_{m=1}^{n_i}$ are weights chosen so that the approximation is exact for polynomials of degree $2n_i - 1$.

The Clenshaw-Curtis integration rule is another choice for the one-dimensional formula $\mathcal{U}_j^i$. In this case, the $\{y_m^i\}_{m=1}^{n_i}$ would be Clenshaw-Curtis points, which can be found, along with the corresponding weights, in ([29]). The Clenshaw-Curtis points possess the attractive quality of *nestedness* for certain choices of n_i. In other words, point sets of increasing order are nested within each other. This leads to an overall decrease in computational effort. (See the references [27], [28], [29] and others for more detail on the Clenshaw-Curtis quadrature).

The one-dimensional interpolant serves as a building block for the Smolyak formula, as we will see soon. In this work we choose $n_1 = 1$ and $n_i = 2^{i-1} + 1$, so that the Clenshaw-Curtis point sets are indeed nested, which reduces the number of points used in total. The Smolyak $N-$dimensional cubature operator is defined as follows:

$$\sum_{s-N+1 \leq |\mathbf{i}| \leq s} (-1)^{s-|\mathbf{i}|} \begin{pmatrix} N-1 \\ s-|\mathbf{i}| \end{pmatrix} \cdot (\mathcal{U}_1^{i_1} \otimes \cdots \otimes \mathcal{U}_N^{i_N}),$$

approximating the N-dimensional integral

$$\int_\Gamma v(\boldsymbol{y})d\boldsymbol{y}.$$

for smooth functions $v : \Gamma \to \mathbb{R}$. The summation is over N-dimensional vectors $\mathbf{i}$ with components $i_1, ..., i_N \in \mathbb{N}$. The parameter s controls the sparseness of the grid; larger s results in more points. The weights for the N-dimensional cubature are combinations of products of the

one-dimensional weights.

We assume that the rule $\mathcal{U}_j^i$ is the same for all dimensions j, so that we can drop the subscript. Let χ^i denote the one dimensional point set used in $\mathcal{U}^i$. The total set of points used in $\mathcal{S}_\Gamma(s)$ is:

$$\mathcal{H}_\Gamma(s) = \bigcup_{s-N+1 \leq |\mathbf{i}| \leq s} (\chi^{i_1} \times \cdots \times \chi^{i_N}).$$

Then, in the general notation we have used above, the collocation points are given by $\{\boldsymbol{q}_j\}_{j=1}^r$ where each $\boldsymbol{q}_j \in \mathcal{H}_\Gamma(s)$ and the total number of points $r = \text{Card}(\mathcal{H}_\Gamma(s))$. When Clenshaw-Curtis one-dimensional rules are used with this choice of n_i, the point sets are nested (i.e. $\chi^{i-1} \subset \chi^i$). When using nested one-dimensional rules the Smolyak formula is actually interpolatory (see [27] for details).

We choose the quadrature rule in each element based on the needs of the problem. The quadrature rule and total number of points need not be the same for all elements. In practice, the choice of what type of approximation to use should be problem-dependent, and factors to take into consideration include: regularity of the integrand and robustness of the rule, preference for points on or off boundaries, and of course the number of points required to achieve a particular degree of exactness. This last consideration is addressed in detail in ([28]). Since nested quadrature rules require less overall points in the Smolyak algorithm, the Clenshaw-Curtis rule is often an attractive choice.

6.3 Connection to gradient-based methods

In this section we make some mathematical connections between ME-PCM local variance-based sensitivity techniques and gradient-based methods. Let us focus on a particular hypercube element B, written without loss of generality as the product set $\prod_{i=1}^N [x_{0,i} - h, x_{0,i} + h]$ where $\boldsymbol{x_0} = (x_{0,1}, x_{0,2}, ..., x_{0,N})$ is the center of B. Suppose we have a function $f \in C^3(B)$ and assume let X is a random variable uniformly distributed on B. We will show that the variance of $f(X)$ over B^i, when normalized with the one-dimensional uniform distribution variance, approximates the norm of the gradient $\|\nabla f|_{\boldsymbol{x}_0}\|^2$ in the limit as $h \to 0^+$. This result is easily generalizable to rectangular B, but we will assume uniform edge lengths for simplicity here.

We begin with the multi-dimensional Taylor expansion:

$$\begin{aligned} f(\boldsymbol{x}) &= f(\boldsymbol{x}_0) + \sum_{|\boldsymbol{\alpha}|=1} \left.\frac{\partial^{\boldsymbol{\alpha}} f}{\partial \boldsymbol{x}^{\boldsymbol{\alpha}}}\right|_{\boldsymbol{x}_0} (\boldsymbol{x}-\boldsymbol{x}_0)^{\boldsymbol{\alpha}} + \frac{1}{2!} \sum_{|\boldsymbol{\alpha}|=2} \left.\frac{\partial^{\boldsymbol{\alpha}} f}{\partial \boldsymbol{x}^{\boldsymbol{\alpha}}}\right|_{\boldsymbol{x}_0} (\boldsymbol{x}-\boldsymbol{x}_0)^{\boldsymbol{\alpha}} \\ &\quad + \frac{1}{3!} \sum_{|\boldsymbol{\alpha}|=3} \left.\frac{\partial^{\boldsymbol{\alpha}} f}{\partial \boldsymbol{x}^{\boldsymbol{\alpha}}}\right|_{\boldsymbol{x}_0} (\boldsymbol{x}-\boldsymbol{x}_0)^{\boldsymbol{\alpha}} + O(\boldsymbol{x}-\boldsymbol{x}_0)^4, \end{aligned} \tag{11}$$

where $\boldsymbol{\alpha}$ is a multiindex of dimension N. In other words, $\boldsymbol{\alpha} = (\alpha_1, \alpha_2, ..., \alpha_N)$, $\alpha_i \in \mathbb{N}$, and $|\boldsymbol{\alpha}| = \alpha_1 + \cdots + \alpha_N$. Let $\int_{\boldsymbol{x}_0-h}^{\boldsymbol{x}_0+h} f(\boldsymbol{x})d\boldsymbol{x}$ denote the N-dimensional integral of f over B. Then,

$$\begin{aligned} & \frac{1}{(2h)^N} \int_{\boldsymbol{x}_0-h}^{\boldsymbol{x}_0+h} f(\boldsymbol{x})d\boldsymbol{x} \qquad (12) \\ = \; & \frac{1}{(2h)^N} \int_{\boldsymbol{x}_0-h}^{\boldsymbol{x}_0+h} \left[f(\boldsymbol{x}_0) + \sum_{|\boldsymbol{\alpha}|=1} \left.\frac{\partial^{\boldsymbol{\alpha}} f}{\partial \boldsymbol{x}^{\boldsymbol{\alpha}}}\right|_{\boldsymbol{x}_0} (\boldsymbol{x}-\boldsymbol{x}_0)^{\boldsymbol{\alpha}} + \frac{1}{2!} \sum_{|\boldsymbol{\alpha}|=2} \left.\frac{\partial^{\boldsymbol{\alpha}} f}{\partial \boldsymbol{x}^{\boldsymbol{\alpha}}}\right|_{\boldsymbol{x}_0} (\boldsymbol{x}-\boldsymbol{x}_0)^{\boldsymbol{\alpha}} \right. \\ & \left. + \frac{1}{3!} \sum_{|\boldsymbol{\alpha}|=3} \left.\frac{\partial^{\boldsymbol{\alpha}} f}{\partial \boldsymbol{x}^{\boldsymbol{\alpha}}}\right|_{\boldsymbol{x}_0} (\boldsymbol{x}-\boldsymbol{x}_0)^{\boldsymbol{\alpha}} + \mathcal{O}(\boldsymbol{x}-\boldsymbol{x}_0)^4 \right] d\boldsymbol{x} \\ = \; & f(\boldsymbol{x}_0) + \frac{1}{2} \sum_{i=1}^{N} \left.\frac{\partial^2 f}{\partial x_i^2}\right|_{\boldsymbol{x}_0} \frac{1}{(2h)^N} (2h)^{N-1} \int_{x_{0,i}-h}^{x_{0,i}+h} (x_i - x_{0,i})^2 dx_i + \mathcal{O}(h^4) \\ = \; & f(\boldsymbol{x}_0) + \frac{1}{2} \sum_{i=1}^{N} \left.\frac{\partial^2 f}{\partial x_i^2}\right|_{\boldsymbol{x}_0} \frac{1}{2h} \frac{2h^3}{3} + \mathcal{O}(h)^4 \\ = \; & f(\boldsymbol{x}_0) + \sum_{i=1}^{N} \left.\frac{\partial^2 f}{\partial x_i^2}\right|_{\boldsymbol{x}_0} \frac{h^2}{6} + \mathcal{O}(h^4) := \mathbb{E}_B[f(X)]. \end{aligned}$$

Using this result,

$$\begin{aligned} \frac{1}{(2h)^N} \int_{\boldsymbol{x}_0-h}^{\boldsymbol{x}_0+h} f(\boldsymbol{x})^2 d\boldsymbol{x} &= f(\boldsymbol{x}_0)^2 + \sum_{i=1}^{N} \frac{h^2}{6} \left(2 \left.\frac{\partial f}{\partial x_i}\right|_{\boldsymbol{x}_0}^2 + 2f(\boldsymbol{x}_0) \left.\frac{\partial^2 f}{\partial x_i^2}\right|_{\boldsymbol{x}_0} \right) + \mathcal{O}(h^4) \\ &:= \mathbb{E}_B[f(X)^2]. \end{aligned}$$

Then we obtain the variance of f over the element B:

$$\begin{aligned}
\mathrm{Var}_B[f(X)] &= \mathbb{E}_B[f(X)^2] - \mathbb{E}_B[f(X)]^2 \\
&= f(\boldsymbol{x}_0)^2 + \sum_{i=1}^{N} \frac{h^2}{6} \left(2 \left.\frac{\partial f}{\partial x_i}\right|_{\boldsymbol{x}_0}^2 + 2f(\boldsymbol{x}_0) \left.\frac{\partial^2 f}{\partial x_i^2}\right|_{\boldsymbol{x}_0} \right) \\
&\quad -f(\boldsymbol{x}_0)^2 - \sum_{i=1}^{N} f(\boldsymbol{x}_0)^2 \left.\frac{\partial^2 f}{\partial x_i^2}\right|_{\boldsymbol{x}_0} \frac{h^2}{3} + \mathcal{O}(h^4) \\
&= \sum_{i=1}^{N} \frac{h^2}{3} \left.\frac{\partial f}{\partial x_i}\right|_{\boldsymbol{x}_0}^2 + \mathcal{O}(h^4) \\
&= \frac{h^2}{3} \|\nabla f|_{\boldsymbol{x}_0}\|^2 + \mathcal{O}(h^4).
\end{aligned}$$

Note that $\frac{h^2}{3}$ is the variance of the one-dimensional distribution of the underlying variable X, and

$$\frac{\mathrm{Var}_B[f(X)]}{\frac{h^2}{3}} = \|\nabla f|_{\boldsymbol{x}_0}\|^2 + \mathcal{O}(h^2).$$

The rate of convergence here is $\mathcal{O}(h^2)$ which is independent of N.